Classical low-coherence interferometry based on broadband parametric fluorescence and amplification

Julien Le Gouët*, Dheera Venkatraman, Franco N. C. Wong and Jeffrey H. Shapiro

Research Laboratory of Electronics, Massachusetts Institute of Technology, 77 Massachusetts Avenue, Cambridge, Massachusetts 02139

*le_gouet@mit.edu

Abstract: We demonstrate that single-mode broadband amplified spontaneous parametric downconversion, combined with optical parametric amplification, can be used as a classical source of phase-sensitive cross-correlated beams. We first study the single spatial mode emission and the spectral brightness properties of the parametric fluorescence, produced in periodically poled MgO-doped lithium niobate. Using the same single-pass bulk-crystal configuration for a pulsed optical parametric amplifier, we achieve a gain of ∼20 dB at an average pump power of 2 W, and explain the pulse narrowing observed at the output of both parametric fluorescence and amplification in the regime of high gain. Combining these two nonlinear processes, we measured optical coherence tomography signals with standard InGaAs photodiodes, thus realizing the first classical interferometer based on amplified parametric fluorescence. The results suggest their utility for demonstrating phase-conjugate optical coherence tomography.

OCIS codes: (190.4410) Nonlinear optics, parametric processes; (190.5040) Phase conjugation; (110.4500) Optical coherence tomography.

References and links

1. W. H. Louisell, A. Yariv, and A. E. Siegman, "Quantum fluctuations and noise in parametric processes. I.," Phys. Rev. **124**, 1646 (1961)
2. D. N. Klyshko, "Coherent photon decay in a nonlinear medium," Sov. Phys. JETP Lett. **6**, 23 (1967).
3. S. A. Harris, M. K. Oshman, and R. L. Byer, "Observation of tunable optical parametric fluorescence," Phys. Rev. Lett. **18**, 732 (1967).
4. D. Magde and H. Mahr, "Study in Ammonium Dihydrogen Phosphate of spontaneous parametric interaction tunable from 4400 to 16 000 Å," Phys. Rev. Lett. **18**, 905 (1967).
5. S. A. Akhmanov, O. N. Chunaev, V. V. Fadeev, R. V. Khokhlov, D. N. Klyshko, A. I. Kovrigin, and A. S. Piskarskas, "Parametric generators of light," Proc. Symposium on Modern Optics, NY (1967).
6. R. L. Byer and S. E. Harris, "Power and bandwidth of spontaneous parametric emission," Phys. Rev. **168**, 1064–1068 (1968).
7. D. C. Burnham and D. L. Weinberg, "Observation of simultaneity in parametric production of optical photon pairs," Phys. Rev. Lett. **25**, 84 (1970).
8. C. K. Hong, Z. Y. Ou, and L. Mandel, "Measurement of subpicosecond time intervals between two photons by interference," Phys. Rev. Lett. 59, 2044 (1987).
9. P. R. Tapster, J. G. Rarity, and J. S. Satchell, "Use of parametric down-conversion to generate sub-Poissonian light," Phys. Rev. A **37**, 2963 (1988).
10. P. Baldi, M. Sundheimer, K. El Hadi, M. P. de Micheli, and D. B. Ostrowsky, "Comparison between difference-frequency generation and parametric fluorescence in quasi-phase-matched lithium niobate stripe waveguides," IEEE J. Sel. Top. Quant. Elec **2**, 385–395 (1996).

#113292 - $15.00 USD Received 24 Jun 2009; revised 14 Aug 2009; accepted 16 Sep 2009; published 22 Sep 2009

11. L. Carrion and J.-P. Girardeau-Montaut, "Development of a simple model for optical parametric generation," J. Opt. Soc. Am. B **17**, 78–83 (2000).
12. D. Ljunggren and M. Tengner, "Optimal focusing for maximal collection of entangled narrow-band photon pairs into single-mode fibers," Phys. Rev. A **72,** 062301 (2005).
13. S. Fasel, O. Alibart, S. Tanzilli, P. Baldi, A. Beveratos, N. Gisin, and H. Zbinden, "High-quality asynchronous heralded single-photon source at telecom wavelength," New J. Phys. **6**, 163 (2004).
14. T. B. Pittman, B. C. Jacobs, and J. D. Franson, "Heralding single photons from pulsed parametric down-conversion," Optics Commun. **246**, 545–550 (2005).
15. C. Kurtsiefer, M. Oberparleiter, and H. Weinfurter, "High-efficiency entangled photon pair collection in type-II parametric fluorescence," Phys. Rev. A **64,** 023802 (2001).
16. F. N. C. Wong, J. H. Shapiro, and T. Kim, "Efficient generation of polarization-entangled photons in a nonlinear crystal," Laser Phys. **16,** 1517–1524 (2006).
17. T. Zhong, F. N. C. Wong, T. D. Roberts, and P. Battle, "High performance photon-pair source based on a fiber-coupled periodically poled $KTiOPO_4$ waveguide," Opt. Express **17**, 12019–12030 (2009)
18. S. Lin and T. Suzuki, "Tunable picosecond mid-infrared pulses generated by optical parametric generation/amplification in $MgO:LiNbO_3$ crystals," Opt. Lett. **21**, 579–581 (1996)
19. Y. Pu, J. Wu, M. Tsang, and D. Psaltis, "Optical parametric generation in periodically poled $KTiOPO_4$ via extended phase matching," Appl. Phys. Lett. **91**, 131120 (2007).
20. N. Mohan, O. Minaeva, G. N. Gol'tsman, M. B. Nasr, B. E. A. Saleh, A. Sergienko, and M. C. Teich, "Photon-counting optical coherence-domain reflectometry using superconducting single-photon detectors," Opt. Express **16,** 18118 (2008).
21. D. Huang, E. A. Swanson, C. P. Lin, J. S. Schuman, W. G. Stinson, W. Chang, M. R. Hee, T. Flotte, K. Gregory, C. A. Puliafito, and J. G. Fujimoto, "Optical coherence tomography," Science **254,** 1178–1181 (1991).
22. B. I. Erkmen and J. H. Shapiro, "Phase-conjugate optical coherence tomography," Phys. Rev. A **74,** 041601(R) (2006).
23. F. A. Bovino, P. Varisco, A. M. Colla, G. Castagnoli, G. Di Giuseppe, and A. V. Sergienko, "Effective fiber-coupling of entangled photons for quantum communication," Opt. Commun. **227,** 343–348 (2003).
24. R. S. Bennink, Y. Liu, D. D. Earl, and W. P. Grice, "Spatial distinguishability of photons produced by spontaneous parametric down-conversion with a focused pump," Phys. Rev. A **74,** 023802 (2006).
25. A. Fedrizzi, T. Herbst, A. Poppe, T. Jennewein, and A. Zeilinger, "A wavelength-tunable fiber-coupled source of narrowband entangled photons," Opt. Express **15,** 15377–15386 (2007).
26. G. D. Boyd and D. A. Kleinman, "Parametric interaction of focused Gaussian light beams," J. Appl. Phys. **39,** 3597–3639 (1968).
27. O. Kuzucu, F. N. C. Wong, D. E. Zelmon, S. M. Hegde, T. D. Roberts, and P. Battle, "Generation of 250 mW narrowband pulsed ultraviolet light by frequency quadrupling of an amplified erbium-doped fiber laser," Opt. Lett. **32,** 1290–1292 (2007).
28. D. E. Zelmon, D. L. Small, and D. Jundt, "Infrared corrected Sellmeier coefficients for congruently grown lithium niobate and 5 mol.% magnesium oxide-doped lithium niobate," J. Opt. Soc. Am. B **14,** 3319–3322 (1997).
29. R. L. Byer, "Parametric oscillators and nonlinear materials," in *Nonlinear Optics*, pp. 47–160, P. G. Harper and B. S. Wherrett, eds. (Academic Press, New York, 1977).
30. B. Lai, N. C. Wong, and L. K. Cheng, "Continuous-wave tunable light source at 1.6 μm by difference-frequency mixing in $CsTiOAsO_4$," Opt. Lett. **20,** 1779–1781 (1995).
31. R. W. Boyd, *Nonlinear Optics, 2nd ed.* (Academic, 2003).

1. Introduction

Parametric fluorescence, or spontaneous parametric downconversion (SPDC), was predicted [1, 2] and observed [3, 4, 5] in the 1960's, and has been extensively studied since then [6, 7, 8, 9, 10, 11, 12]. More recently, SPDC has been notably used as a source of heralded single photons [13, 14] or entangled pairs of photons [15, 16, 17], and has therefore been the workhorse of quantum interferometry. These results are based on the quantum properties that appear in a regime of low energy pumping. On the other hand, other works have been dedicated to extract the highest optical conversion efficiency [18, 19], from the pump to the generated beams, in order to generate strong frequency-shifted beams, without the need of an external cavity, as in optical parametric oscillators.

Weakly pumped SPDC has been utilized in a classical interference experiment with photon-counting measurements using superconducting single-photon detectors. [20]. However, none of this prior work has exhibited the classical phase coherence of signal and idler beams, gen-

#113292 - $15.00 USD Received 24 Jun 2009; revised 14 Aug 2009; accepted 16 Sep 2009; published 22 Sep 2009

erated in a strong pumping regime, by means of interference measurements. Here we report the demonstration of such interference. In particular, we take advantage of the phase coherence of an amplified parametric fluorescence source and an optical parametric amplifier to realize a standard optical coherence tomography (OCT) experiment [21].

By strongly pumping our type-0 nonlinear crystal, we realize an ultrabroadband SPDC source with a 132 nm phase-matching bandwidth centered at 1560 nm. In this spectrum, we select two narrow spectral lines at 1550 nm and at 1570 nm, which are generated in a single spatial mode with a single-mode generation efficiency of about 70%. The 1550 nm beam, playing the role of the reference, is sent through a delay line. The 1570 nm beam, the signal, illuminates a sample to interrogate its reflectivity. The reflected fraction of the signal is then sent to an optical parametric amplifier (OPA), to generate an amplified and phase-conjugated beam. The amplification overcomes the losses in the signal path transmission, whereas the phase-conjugation generates an output beam at the same wavelength as the reference beam. Finally, the conjugated signal beam is recombined with the reference for the interference measurement, using standard InGaAs photodetectors. To our knowledge, this is the first demonstration of an interferometer based on amplified parametric fluorescence as a classical coherent source. We believe that our combination of SPDC and an OPA will allow us to realize the phase-conjugate optical coherence tomography [22], in which the signal interrogates the sample twice, with a phase conjugation after the first reflection. The double-pass configuration is predicted to yield a factor-of-two axial resolution improvement, and the phase conjugation inverts the spectral phase to compensate even-order dispersion in the propagation medium.

In Sec. 2 we describe the operation and characterization of amplified SPDC as a single-mode fiber-coupled coherent source under strong pulsed pumping. Section 3 details the gain measurements of our strongly pumped OPA with inputs from a weak continuous-wave (cw) laser and from the signal beam of the amplified SPDC source. We will then describe our standard OCT measurements using the amplified SPDC source and the OPA in Sec. 4 before concluding in Sec. 5.

2. Amplified parametric fluorescence

To generate signal and idler outputs that behave classically, one must operate SPDC under strong pumping in a high photon-flux regime, with many photons per output pulse, such that standard photodetectors can be used. We chose periodically poled MgO-doped lithium niobate (PP-MgO:LN) as the nonlinear material to take advantage of the large nonlinear coefficient d_{33} in type-0 phase matching in which the pump, signal, and idler are polarized along the crystal's z axis. Our $20\times3\times0.5\,\mathrm{mm}^3$ (L $\times$ W $\times$ H) PP-MgO:LN crystal from HC Photonics had a grating period $\Lambda = 19.47\mu$m designed for degenerate SPDC operation pumped at 780 nm. Even though the SPDC output is generally multi-spatial-mode, it is much more useful to operate in a single spatial mode for more efficient fiber-optic transmission, phase conjugation, amplification, and interferometric measurements. In this Section, we will describe our efforts in producing SPDC in a mostly single spatial mode fashion by optimal pump focusing, and report the results of our characterization of the broadband outputs under strong pumping.

2.1. Single-mode parametric fluorescence

SPDC is utilized in many applications in the fields of nonlinear optics and quantum information science. Recently a number of theoretical and experimental studies have been dedicated to the problem of modifying the typical multimode output of SPDC so that most of the output is in a single spatial mode [12, 15, 23, 24, 25]. The basic idea is that a plane-wave pump excites many spatial modes and therefore a focused pump beam can concentrate the output into a single spatial mode, that can be efficiently coupled into a single-mode fiber. While the calculations

#113292 - $15.00 USD Received 24 Jun 2009; revised 14 Aug 2009; accepted 16 Sep 2009; published 22 Sep 2009

in the previous references are based on spontaneous emission, their results are quite similar to the optimal focusing parameter calculated by Boyd and Kleinman for single-mode three-wave mixing interactions with well-defined input spatial modes [26]. Boyd and Kleinman found that the output power is maximized if the focusing parameter $\xi = L/b = 2.84$, where L is the crystal length, $b = 2n\pi w_0^2/\lambda$ is the confocal parameter in the crystal, w_0 is the beam waist, and n is the crystal's index of refraction at the vacuum wavelength λ.

For collinearly propagating SPDC in a bulk nonlinear crystal, numerical calculations by Ljunggren and Tengner suggest that the optimal focusing parameters should be $0.5 \leq \xi_p \leq 1$ for the pump, and $1 \leq \xi_t \leq 1.5$ for the output signal and idler [12], as confirmed recently in a type-II collinearly phase-matched experiment [25]. Note that ξ_p and ξ_t are not equal, whereas in Boyd and Kleinman's calculation, the confocal parameters for all three fields (pump, signal, idler) are the same for optimal output.

There are three main contributions to the phase-matching condition and therefore the spatial mode distribution of the output. First, there is the natural divergence of the generated fields due to the finite crystal length under plane-wave pumping. For degenerate SPDC, the transverse momenta for the signal and idler are equal and opposite such that $\theta_s = -\theta_i$, where $\theta_{s,i}$ is the angle between the signal (idler) wave vector and the plane-wave pump propagation axis, which we assume to be along a principal axis of the crystal. The longitudinal phase matching condition then becomes

$$\Delta k_z(\theta_{s,i}) = k_p - k_s \cos\theta_s - k_i \cos\theta_i - \frac{2\pi}{\Lambda} = k_s \theta_s^2 \,, \tag{1}$$

where perfect phase matching is assumed in the collinear direction, $\Delta k_z(0) = 0$, and we note that $k_s = k_i$ for degenerate type-0 phase matching. The output power is proportional to $\mathrm{sinc}^2(\Delta k_z L/2)$ and it is convenient to define the phase-matching bandwidth by the condition

$$\Delta k L = \pi \,. \tag{2}$$

The natural divergence of the signal and idler fields is then given by the internal angles

$$\bar{\theta}_{s,i} = \sqrt{\frac{\pi}{k_s L}} = \sqrt{\frac{\lambda_s}{2n_s L}} \,. \tag{3}$$

The second phase-matching contribution is from a focused pump beam, with an internal pump divergence angle $\theta_p = \lambda_p/\pi n_p w_p$. For small θ_p, the pump focusing creates an angular spread of the signal and idler outputs with the same magnitude as θ_p. The third contribution is from the signal and idler measurement spectral bandwidth. For a measurement bandwidth small compared with the phase-matching bandwidth, as in our case, this contribution to the divergence angle is negligible.

One can argue that the optimal pump focusing, in terms of single-mode generation of the fluorescence, is obtained by equalizing the divergence angle due to pump focusing and the natural divergence angle: $\theta_p = \bar{\theta}_s$. Indeed, by considering the natural divergence angle as the angular spread of a single spatial mode, one see that this equality allows us to concentrate most of the emission in a single spatial mode. In other words, the pump is focused to a spot that supports only a single spatial mode of the signal and idler. It is then easy to show that the pump focusing parameter is $\xi_p = \pi/2 \approx 1.6$. For collection of the generated beams, the output divergence is given by the root sum square of the two independent contributions from pump focusing and natural divergence: $\theta_t = \sqrt{\bar{\theta}_s^2 + \theta_p^2} = \sqrt{2}\theta_p$. This corresponds to a target (signal or idler) focusing parameter $\xi_t = \xi_p$.

Compared with the calculations of Ljunggren and Tengner [12], our simple arguments yield a pump focusing parameter ξ_p that is slightly larger than their suggested range, but close enough

#113292 - $15.00 USD Received 24 Jun 2009; revised 14 Aug 2009; accepted 16 Sep 2009; published 22 Sep 2009

that we consider $0.5 \leq \xi_p \leq 1.5$ as a good starting range for our experiment. Interestingly, our last argument about pump and target focusing parameters leads to the same conclusion as in [26] ($\xi_p = \xi_t$), whereas the calculations in [12] indicate that the output ξ_t is 1.5 to 2 times larger than ξ_p. We believe the difference may be due to the measurement bandwidth. In our case, the measurement bandwidth is much smaller than the phase-matching bandwidth and therefore it has no influence on the emission spatial mode. Typically, however, the measurement and phase-matching bandwidths are comparable and a broader emission angular spread is expected. A larger effective angular spread yields a smaller confocal parameter and hence a larger ξ_t. As mentioned below, our experimental optimization confirms that $\xi_p \sim \xi_t$.

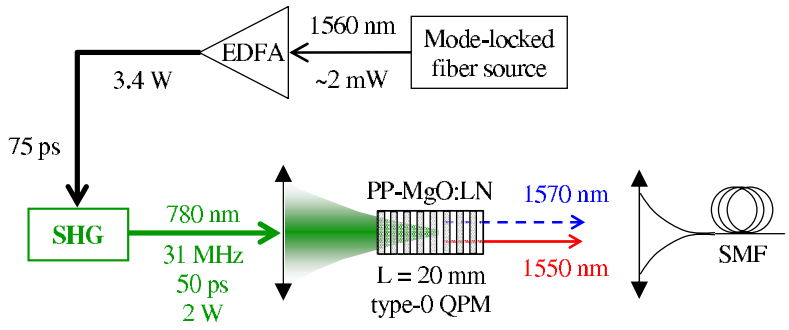

Fig. 1. Schematic of setup for parametric fluorescence generation and single-mode fiber collection, using a type-0 quasi phase-matching (QPM): pump, signal and idler are polarized on the same axis. The pulsed pump source at 780 nm is based on a passively mode-locked fiber laser, an erbium doped fiber amplifier (EDFA), and single-pass second-harmonic generation (SHG).

Figure 1 shows a schematic of the SPDC generation and collection setup. A mode-locked fiber laser at 1560 nm used an erbium-doped polarization-maintaining (PM) fiber as the lasing medium and a free-space saturable absorbing mirror for passive mode locking [27]. The center wavelength was set by a fiber Bragg grating within the laser cavity. The fiber laser generated 1.9 mW of 75-ps transform-limited pulses at a repetition rate of 31.1 MHz, and the output was amplified by a 5-W IPG Photonics PM erbium-doped fiber amplifier (EDFA). We frequency doubled the EDFA output by second-harmonic generation (SHG) in a 10-mm-long PP-MgO:LN crystal to yield ~50-ps pulses at 780 nm that served as the SPDC pump source. The PP-MgO:LN SHG crystal had the same grating period (19.47 μm) as the SPDC and OPA crystals, all operating at a temperature of 86.5° C. We focused the infrared (IR) beam to a waist of 40 μm and obtained a SHG conversion efficiency of 59%, converting 3.4 W of input IR power into 2 W output at 780 nm. No crystal damage was observed. After the SHG crystal a set of dichroic mirrors were used to reject most of the remaining 1560-nm pump with only ~1 nW of residual power at the input to the SPDC crystal. We optimized the alignment of the SPDC crystal and the 780-nm pump so that no residual 1560-nm light after the SPDC crystal was coupled into the single-mode fiber.

We optimized the pump focusing for the SPDC crystal by maximizing the total SPDC output that could be coupled into a single-mode fiber. The percentage η_{SM} of the total SPDC output in a single spatial mode is obtained by measuring the ratio between the powers respectively at the outputs of single-mode and multi-mode fibers, and is corrected for the reflection loss at the input of the multi-mode fiber. Taking into account the fiber coupling efficiency η_f into the single-mode optical fiber (anti-reflection coated), the effective single-mode SPDC coupling

#113292 - $15.00 USD Received 24 Jun 2009; revised 14 Aug 2009; accepted 16 Sep 2009; published 22 Sep 2009

efficiency is $\eta_T = \eta_{SM}\eta_f$. To limit the collected SPDC to a bandwidth small compared with the phase-matching bandwidth, the output of the fiber was transmitted through a 5-nm interference filter (Andover, Inc.) centered at 1551 nm. We first chose a pump waist $w_p = 35$ μm for a focusing parameter $\xi_p \approx 1$. We collected the total SPDC output by coupling it into a multi-mode fiber and measured the power using an InGaAs detector with a 10-fW detection sensitivity. We then optimized the collection optics for coupling into a single-mode fiber and measured the single-mode power with the same detector.

With the initial setting ($\xi_p = \xi_t \sim 1$), we obtained $\eta_T = 50\%$. In a separate measurement, using a 1550 nm laser source, we usually obtain a single-mode fiber coupling efficiency $\eta_f = 82 \pm 2\%$. Therefore, we can reasonably deduce that the single-mode content of the SPDC output was $\eta_{SM} = 61 \pm 1.5\%$. We then varied the pump focusing, and at each pump focus setting we optimized the collection into the single-mode fiber. Reducing the pump waist to $w_p = 25$ μm and optimizing the focal length of the collection optics (that leads to $\xi_p = \xi_t = 1.7$), we obtained $\eta_T = 57.5\%$ which corresponds to a single-mode SPDC output ratio $\eta_{SM} = 70 \pm 2\%$. We did not try to focus the pump beam tighter than $w_p = 25\mu$m to avoid potential crystal damage. In a similar experiment concerned with optimization of pump focusing, in type-II phase-matched periodically poled $KTiOPO_4$, Fedrizzi *et al.* found that the optimal pump focusing parameter lies in a range $0.9 \leq \xi_p \leq 1.3$ and $\xi_t \sim 1.6$ [25]. The small difference between our measured values and those of Fedrizzi *et al.* can be attributed to the much smaller ratio of our collection bandwidth relative to the phase-matching bandwidth.

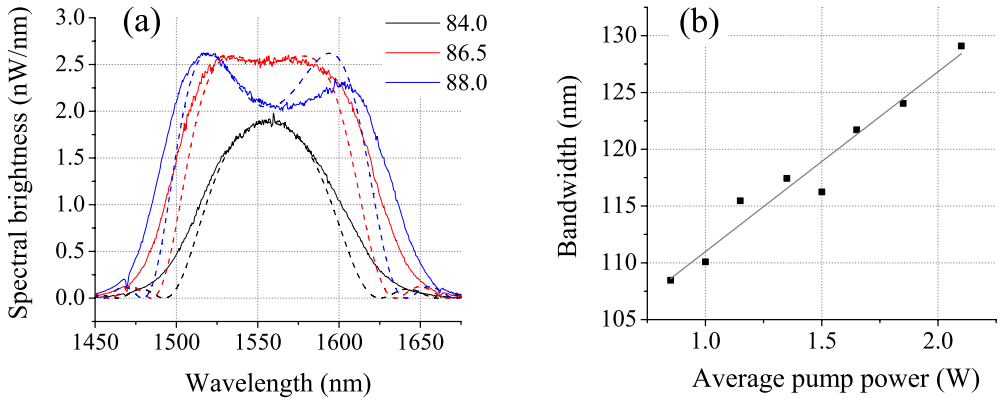

Fig. 2. (a) Power spectral densities (solid lines) of SPDC output collected in a single-mode fiber at a pump power of 2 W, for various crystal temperatures. Theoretical models (dashed lines) are obtained by calculating the phase-matching function using Sellmeier coefficients. (b) Linear dependence of the spectral bandwidth as a function of the pump power, at a crystal temperature of 86°C. The solid line is the fit of the data points.

2.2. Spectral bandwidth and brightness

Figure 2(a) shows the single-mode fiber-coupled SPDC output spectra (solid lines) that we measured with an optical spectrum analyzer at different crystal temperatures, for a pump power of 2 W. We conveniently define the bandwidth using Eq. (2), so it corresponds to the full width at 40% maximum. The measured spectral bandwidths at 84°C, 86.5°C and 88°C are respectively 100, 132, and 150 nm. For these measurements, the fluorescence brightness at 1550 and 1570 nm was maximum at 86.5°C. Figure 2(b) shows the variation of the bandwidth

#113292 - $15.00 USD Received 24 Jun 2009; revised 14 Aug 2009; accepted 16 Sep 2009; published 22 Sep 2009

with the pump power, at a constant temperature of 86°C.

The phase-matching function of Eq. (1), for collinear plane waves, can be calculated using the Sellmeier coefficients [28] supplied by the crystal's manufacturer, including the temperature dependence of the refractive indices. When inserting the total phase mismatch into the well-known formula for the output power $P(\lambda_s) \propto \mathrm{sinc}^2[\Delta k(\lambda_s)L/2]$ [6], we obtain the dashed curves, whose bandwidths are 85, 114, and 126 nm for respectively 84°C, 86.5°C and 88°C. Calculated and measured bandwidths are thus in reasonable. The slight difference (about 15%) can be due to inaccurate Sellmeier coefficients or to pump focusing, which modifies the phase-matching condition. Finally, as shown in Fig. 2(b), we measured an increase of the spectral bandwidth of SPDC as a function of the average pump power. The observed bandwidth increase under strong pumping is in good qualitative agreement with the theory of parametric amplification [29].

Because we are primarily interested in exploiting the phase-sensitive cross correlation between the SPDC signal and idler and in obtaining high-flux outputs, it is desirable to have strong pumping beyond the typical regime of linear power dependence. Figure 3 shows the detected SPDC spectral brightness centered at 1560 nm as a function of the average pump power, showing clearly exponential growth due to parametric amplification of parametric fluorescence. The measurement was taken at the output of a single-mode fiber and with a 0.36-nm bandpass filter. At low pump powers, the linear slope is ∼46 pW/nm/W, and the amplified parametric fluorescence reached 1 nW/nm at an average pump power of 1.9 W, which is a factor of 10 higher than the linearly projected brightness.

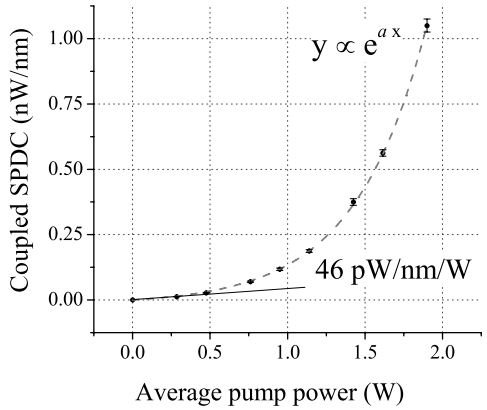

Fig. 3. Spectral brightness of parametric fluorescence measured at the output of a single-mode fiber as a function of average pump power. Dashed line shows exponential fit proportional to $\exp(a\langle P_p\rangle)$ with $a = 2.17 \pm 0.02$.

We can compare the low power measurements with the estimated signal power, according to Byer and Harris [6]:

$$\frac{\mathrm{d}P_s}{\mathrm{d}\lambda_s} = \frac{32\pi^4 d_{\mathrm{eff}}^2 n_s \hbar c}{\varepsilon_0 \lambda_s^6 \lambda_i n_i n_p} L^2 P_p \int_0^{\pi/2} \theta_s \mathrm{sinc}^2 \left[\Delta k(\theta_s)\frac{L}{2}\right] \mathrm{d}\theta_s \,, \tag{4}$$

where P_p is the average pump power. This equation refers to the free-space signal output brightness, at low pump power, that is valid for a plane-wave or focused pump. For a plane-wave pump and assuming perfect phase matching for the collinearly propagating outputs, we have $\Delta k(\theta_s) = k_s \theta_s^2$. We estimate the effective nonlinear coefficient $d_{\mathrm{eff}} = 2d_{33}/\pi = 13$ pm/V, based on a separate second-harmonic generation measurement. For $L = 20$ mm, we evaluate numeri-

#113292 - $15.00 USD Received 24 Jun 2009; revised 14 Aug 2009; accepted 16 Sep 2009; published 22 Sep 2009

cally the spectral brightness given by Eq. (4) to be 139 pW/nm/W for the signal beam. We note that at low powers, there is no difference in the brightness between a cw or pulsed pump for the same average power. Considering that the measured power included both signal and idler, and taking into account $\eta_{\rm SM} = 70\%$, $\eta_f = 82\%$, and a transmission of 30% through the bandpass filter and various optical components, the low-power measurement of Fig. 3 corresponds to a generated signal spectral brightness of 134 pW/nm/W, in excellent agreement with the theoretical estimate. Note that it would have been possible to reach a much higher SPDC brightness by directly pumping the crystal with a femtosecond laser at 780 nm (see for example [19], where an average signal power of 0.49 mW has been achieved in type-II conversion). However we did not have the opportunity to use one for this proof of principle experiment.

3. Optical Parametric Amplification

The second crucial step for implementing the interferometer is the parametric amplification of the returned signal beam. The OPA is used to generate an amplified phase-conjugate signal at the same wavelength as the reference beam so that they can interfere. We implemented the OPA using a second PP-MgO:LN crystal, that is identical to the one used for SPDC. We first characterized the OPA gain under pulsed pumping using a cw input laser. Then we studied the amplification process using the SPDC idler pulses described in Sec. 2 as the input to the OPA.

3.1. OPA with cw input signal

Optical parametric amplification in a nonlinear crystal is simply difference frequency generation under high gain, with a pump photon that has a higher energy than the input signal and the output phase-conjugate idler photons. Energy conservation yields the idler frequency $\omega_i = \omega_p - \omega_s$, and the idler phase is given by $\phi_i = \phi_p - \phi_s$.

In the low gain regime the OPA gain is linearly proportional to the pump power P_p, and, in the nearly degenerate case ($\lambda_s \sim \lambda_i$), is given by [30]

$$g(P_p) = \frac{P_i(L)}{P_s(0)} = \frac{16\pi d_{\rm eff}^2 L\, \bar{h}_m(\xi_p)}{c\varepsilon_0 n_p n_s n_i \lambda_i^2 (1/k_s + 1/k_p)} P_p\,, \tag{5}$$

where $P_s(0)$ and $P_i(L)$ are the input signal and output idler powers, and k_p and k_s are the wave numbers in the crystal of length L. $\bar{h}_m(\xi_p)$ is the reduction factor due to the influence of the focusing parameter ξ_p on three-wave nonlinear mixing without double refraction [26]. In our measurements $\lambda_s = 1570$ nm and $\lambda_i = 1550$ nm, so we can approximate $\lambda_s \approx \lambda_i \approx 2\lambda_p$ and $n_p \approx n_s = n_i = 2.15$, and simplify the linear gain to

$$g(P_p) = \frac{64\pi^2 d_{\rm eff}^2 L\, \bar{h}_m}{3c\varepsilon_0 n_s^2 \lambda_s^3}\, P_p\,, \tag{6}$$

in which we assume optimal pump and signal focusing $\xi_p = \xi_s$. For $L = 20$ mm and a focusing parameter $\xi_p = 1.06$ ($\bar{h}_m \approx 0.8$), we obtain a linear gain coefficient $g(P_p)/P_p$ of $\sim$1.2%/W.

For pulsed pumping, the peak power can easily reach kW levels into the high-gain regime. Under strong pumping, but still assuming no pump depletion, the OPA gain for a plane-wave pump is the well-known formula [31]

$$G(P_p) = \sinh^2\left[\kappa(P_p)L\right], \tag{7}$$

where $\kappa(P_p)$ is the pump power-dependent gain coefficient. Noting that $G(P_p) \underset{\sim}{\to} g(P_p)$ for low pump powers and that $\sinh(x) \to x$ for small x, we include the reduction factor $\bar{h}_m$ in $G(P_p)$ by requiring that $[\kappa(P_p)L]^2 = g(P_p)$.

#113292 - $15.00 USD Received 24 Jun 2009; revised 14 Aug 2009; accepted 16 Sep 2009; published 22 Sep 2009

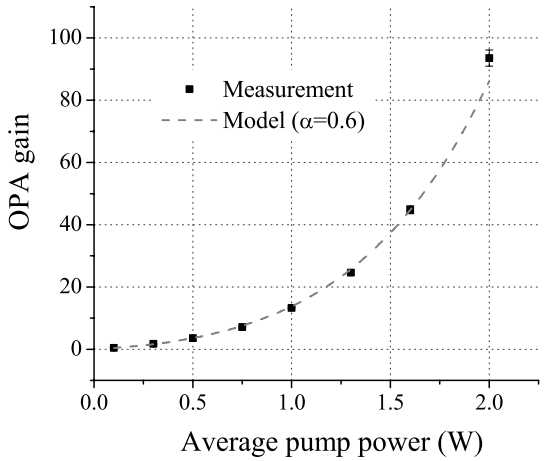

Fig. 4. Measured OPA gain (solid points) and theoretical values (dashed line) as functions of the average pulsed pump power. Experimental data are corrected for filter transmission and single-mode fiber coupling efficiencies, and input signal power is multiplied by the duty cycle ratio τ/T to take into account that the pump was pulsed. The theoretical model is based on Eq. (8) with a fitting factor $\alpha = 0.6$.

To apply Eq. (7) to our pulsed pump operation, we approximate the pump as composed of square pulses of duration τ with period T and average power $\langle P_p \rangle$. The peak power for Eq. (7) is $P_p = \langle P_p \rangle T/\tau$, where τ/T is the duty cycle for the mode-locked pump laser. Furthermore, we allow a fitting factor $\alpha < 1$ to account for nonidealities such as pump pulse broadening (with reduced peak power), mode-matching inefficiency, and our assumption of a square pulse shape. The OPA gain then becomes

$$G(P_p) = \sinh^2\left(\frac{8\pi d_{\text{eff}}}{n_s \lambda_s}\sqrt{\alpha \frac{L\,\bar{h}_m\,\langle P\rangle T}{3c\varepsilon_0 \lambda_s \tau}}\right). \tag{8}$$

The nonlinear PP-MgO:LN crystal for the OPA gain measurement was identical to that used for SPDC measurements. The pump was derived from the same pump laser used for generating the SPDC source, with a mode locking frequency $1/T$ of 31.1 MHz and a nominal pulse width τ of 50 ps. The pump beam focus had a beam waist $w_p = 33\ \mu$m ($b_p = 18.9$ mm), which yields a reduction factor $h_m \approx 0.8$. For the cw signal input, we used a tunable laser (Agilent HP81689A) with a power of 1 mW at 1570 nm. The signal confocal parameter b_s should be closely matched to that of the pump to optimize the nonlinear interaction [26]. In the measurements we set the signal beam waist to $w_s = 40\ \mu$m ($\xi_s = 1.4$), which is not closely matched to the pump focusing parameter $\xi_p = 1.06$. After the crystal, the 1550-nm idler beam was optimally coupled into a single-mode fiber, and separated from the 1570-nm input signal using a coarse wavelength division multiplexer (CWDM) with 16-nm-wide channels centered at 1551 and 1571 nm. The idler output from the 1551-nm channel was then sent through a fiber-coupled 0.36-nm filter centered at 1550 nm before detection by a fiber-coupled InGaAs photodetector (Agilent HP81634A). There was no leakage of the 1571-nm input signal at the detector.

The OPA power gain, using a cw laser at 1570 nm as input, was characterized as a function of the average power of the 780-nm pulsed pump laser, and is shown in Fig. 4. A theoretical fit (dashed curve) to the data using Eq. (8) with a fitting parameter $\alpha = 0.6$ is also displayed. The

#113292 - $15.00 USD Received 24 Jun 2009; revised 14 Aug 2009; accepted 16 Sep 2009; published 22 Sep 2009

reasonably good agreement between data and theory with one adjustable parameter indicates that the measurement methodology is sound and that the functional dependence on the pump power is well understood. More importantly, we have achieved a gain of almost 20 dB for a pump input power of 2 W.

3.2. OPA with pulsed input signal

After optimizing the OPA setup and alignment with the cw input signal, we replaced it with the pulsed input derived from the 1570-nm signal output of the pulsed SPDC described in Sec. 2. The SPDC outputs were coupled into a single-mode fiber and separated into different wavelength channels with the fiber-coupled CWDM. For a pulsed pumped OPA with a pulsed input, it is essential that the pump and input pulses have good temporal overlap at the OPA crystal to optimize the phase-conjugate idler output.

For the pump pulses, we assume a Gaussian shape with a full width at half-maximum (FWHM) $\tau = 50$ ps given by

$$P_p(t) = \bar{P_p} \exp\left(-4\ln 2\,\frac{t^2}{\tau^2}\right), \tag{9}$$

where $\bar{P_p}$ is the peak pump power at $t = 0$. As noted in Fig. 3, the SPDC output power as a function of a given average pump power $\langle P_p \rangle$ scales as $P_s \propto \exp[2.17\langle P_p \rangle]$. Given the shape of a pump pulse, the probability for generating parametric fluorescence should be higher at the center of the pump pulse than in its wings, and therefore, the output SPDC pulse should be narrower than the pump pulse. Analytically, the intensity shape of the SPDC pulses generated by an average pump power $\langle P_{p1} \rangle = 2$ W can be written as:

$$P_s(t) \propto \exp\left[2.17\langle P_{p1}\rangle \times \exp\left(-4\ln 2\,\frac{t^2}{\tau^2}\right)\right] \tag{10}$$

The width of the SPDC output pulses generated by our 2-W pump was thus 25 ps.

The amplitude of the OPA-generated idler field, as a function of the spatial delay z_d between the pump and the probe pulse, is given by the time convolution of the input signal amplitude and the amplitude gain, obtained from Eq. (8). The idler output power is then given by

$$P_i(z_d) = \left[\int \mathrm{d}z\, \sqrt{P_s(z)}\, \sinh\left(\sqrt{\alpha g\,(P_p(z - z_d))}\right)\right]^2, \tag{11}$$

where, for easier comparison with experimental data, we have converted the time variable t into a free-space spatial variable ($z = ct$), and the spatial pulse width is $\delta = c\tau$. Note that we use here the previous fitting factor $\alpha = 0.6$ for the high-gain regime (see Fig. 4).

Figure 5 shows the normalized average idler power as a function of the delay z_d between the pump and input signal pulses, and the theoretical values calculated from Eq. (11). For the measurements, we used an average pump power of 2 W for the SPDC crystal and 1.3 W for the OPA, where an OPA gain of 14 dB was expected according to Fig. 4. The width (FWHM) of the output idler pulse is 50 ps ($\delta = 15$ mm), which is narrower than one would expect from the linear convolution of the input signal pulse (FWHM = 25 ps) and the pump pulse (FWHM = 50 ps). This narrowing is again due to the strong power of the pulsed pump, such that the OPA gain is higher at the center of the idler pulse than in its wings. The good agreement between theory and measurements confirms our model. Figure 5 also indicates the need for synchronizing the pump and input signal pulses within a few millimeters in order to optimize the pulsed parametric amplification process.

#113292 - $15.00 USD Received 24 Jun 2009; revised 14 Aug 2009; accepted 16 Sep 2009; published 22 Sep 2009

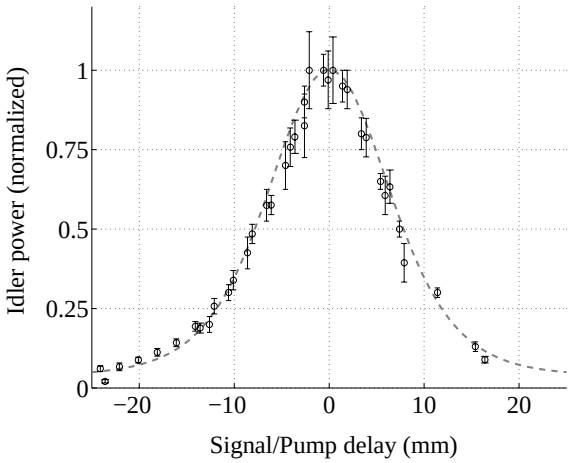

Fig. 5. Normalized idler power as a function of the pump-signal spatial delay and theoretical values (dashed curve) based on Eq. (11). The idler power envelope width (FWHM) is 15 mm ($\tau = 50$ ps).

4. Classical OCT

We illustrated the coherence properties of the SPDC source and OPA combination by demonstrating a standard OCT measurement of a highly reflective target mirror. This single-pass configuration will provide a baseline measurement for a future phase-conjugate OCT experiment, to illustrate its axial resolution enhancement.

Both the SPDC and OPA devices were pumped by the same 50-ps mode-locked laser at 780 nm, thus providing the necessary jitter-free synchronization. Figure 6 shows the schematic for the experimental setup. We used the CWDM to filter the SPDC outputs into separate channels and utilized the light around 1570 nm as the signal and 1550 nm as the reference. The reference pulse was sent through a length of fiber that served as a delay line for pulse overlap synchronization. For fine balancing of the reference length in the OCT interferometer, a free-space delay line was installed using a free-space mirror mounted on an translation stage, and a fiber circulator was used to route the pulse to and from the reference mirror. A 0.36-nm tunable bandpass filter centered at 1550 nm set the reference pulse bandwidth for OCT measurements with a corresponding transform-limited pulse width of $\sim$10 ps. The corresponding free-space coherence length of 3 mm defined the OCT measurement resolution. After the 0.36-nm bandpass filter, the reference pulse was sent to the reference arm of a fiber interferometer composed of a fiber 50-50 beam splitter. The average power of the reference beam at the input of the interferometer was typically 200 pW.

The signal beam from the 1570-nm CWDM channel was sent to the target and the reflected light was routed to the OPA with the use of a circulator composed of a polarizing beam splitter and a quarter-wave plate. The target, mounted on a translation stage, was a highly reflective mirror. The reflected signal was then coupled with the pump to the OPA crystal to generate the amplified phase-conjugate signal at 1550 nm. Another fiber-coupled 0.36-nm tunable bandpass filter was inserted after the OPA to select only the phase-conjugate beam at 1550 nm. After amplification and filtering, the maximum output power of the phase-conjugate signal beam reached 2 nW. Therefore, we had sufficient OPA gain to tolerate losses in the signal path up to 10 dB without compromising the contrast of the interference signal, which requires equal

#113292 - $15.00 USD Received 24 Jun 2009; revised 14 Aug 2009; accepted 16 Sep 2009; published 22 Sep 2009

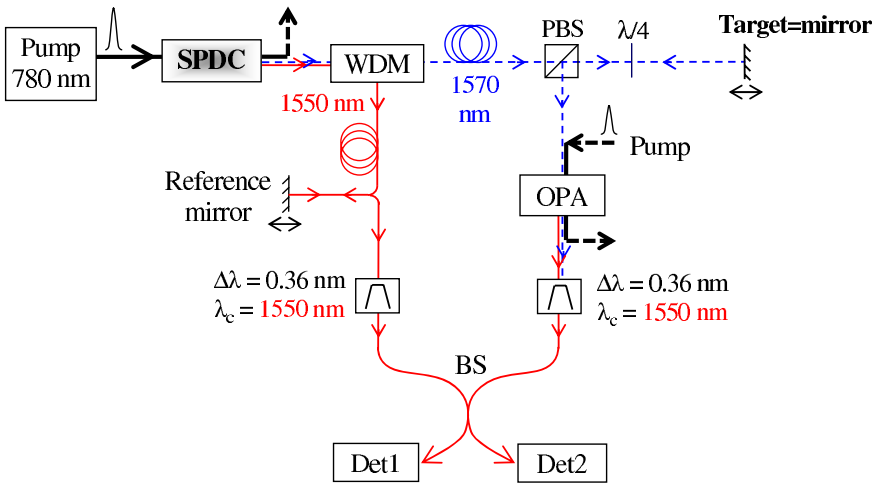

Fig. 6. Schematic of classical OCT experiment. Det, photodetector channels (1 and 2); BS, beam splitter; PBS, polarizing beam splitter; CWDM, coarse wavelength division multiplexer; SPDC, spontaneous parametric downconverter; OPA, optical parametric amplifier.

reference and phase-conjugate input powers.

Because the SPDC signal-idler relative phase can vary from pulse to pulse, stable OCT interference between the signal and reference pulses can occur only if they are derived from the same pump pulse. Therefore, the fiber delay line in the reference path ensured approximately equal lengths for the reference and signal arms. Using the pulsed fiber laser at 1560 nm we were able to measure the path difference between the reference and phase-conjugate beams with an accuracy of a few mm over a distance of 25 m (between the SPDC source and the 50-50 beam splitter). For fine tuning, we adjusted slightly the position of the reference mirror and confirmed the reference and phase-conjugate pulse overlap by observing the interference between the two fields at the output of the 50-50 beam splitter. In the OCT measurement, we were interested in obtaining the interference envelope so it was not necessary to stabilize the interferometer's two long paths. The envelope was obtained by recording the interference signals at the beamsplitter outputs while the path lengths were fluctuating (because of vibrations) by more than a wavelength. Even though the power fluctuations of the reference and signal arms could be relatively important (about 10%), they were exactly common to both beams. Thus we normalized the difference between the two outputs powers by their sum, and got rid of the effect of power fluctuations on the contrast.

Figure 7 shows the contrast of the measured interference signal as a function of the position z_r of the reference mirror, for two positions of the target, $z_T = 300$ mm and 302.35 mm. The dashed lines are based on the following theoretical model. Let us first consider the measurement of the interference envelope at one target position. We have confirmed in a separate measurement that the intensity spectrum of the transmission through the 0.36-nm bandpass filter can be well described by a squared Lorentzian shape

$$T_I(\lambda) = T_I^0 \left[1 + 4\left(\frac{\lambda - \lambda_c}{\Delta\lambda_0}\right)^2\right]^{-2} \tag{12}$$

with $\Delta\lambda_0 = 0.56$ nm, corresponding to the transmission bandwidth FWHM of $\Delta\lambda_F = 0.36$ nm.

#113292 - $15.00 USD Received 24 Jun 2009; revised 14 Aug 2009; accepted 16 Sep 2009; published 22 Sep 2009

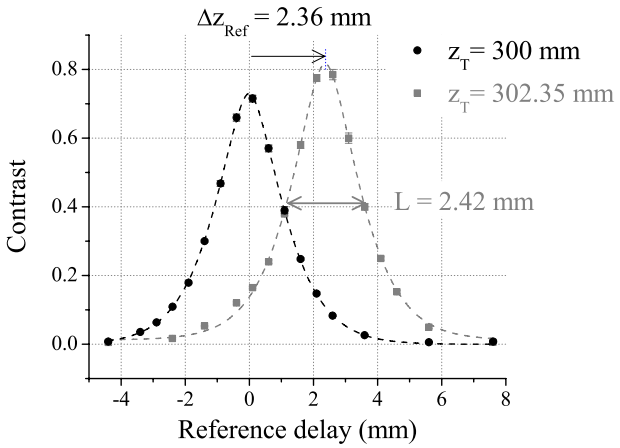

Fig. 7. Contrast of the interference between signal and reference pulses (with equal powers), as a function of the reference mirror position at two target locations z_T. The dashed lines correspond to the theoretical model given by Eq. (14).

From this spectrum expression, we approximate the amplitude envelope of the reference and phase-conjugate signal pulses after the bandpass filters with the following spatial shape

$$\tilde{T}_E(z) = E_0 \, \exp\left(-\pi \frac{\Delta\lambda_0}{\lambda^2}|z|\right), \tag{13}$$

except for the singularity at the peak position $z = 0$, which does not affect the calculations. For two interfering fields with identical amplitudes, the spatial envelope of the interference contrast is described by the following function of the reference delay

$$\begin{aligned} C(z_r) &= \int \mathrm{d}z \, \tilde{T}_E(z)\tilde{T}_E(z-2z_r) \\ &= C_0\left(1+\pi\frac{\Delta\lambda_0}{\lambda^2}|2z_r|\right)\exp\left(-\pi\frac{\Delta\lambda_0}{\lambda^2}|2z_r|\right), \end{aligned} \tag{14}$$

where C_0 is a normalization factor. The factor of 2 for z_r takes into account the fact that the actual delay is twice the position shift z_r of the reference mirror. Applying this model to the measurement in Fig. 7 we find excellent agreement between the calculated interference contrast (dashed lines) and the experimental data (points).

In OCT measurements, interest is in the ability to distinguish the axial positions of different target locations. Thus, we moved the target by an amount equal to $\Delta z_T = 2.35$ mm, as measured with a vernier ruler located at the target translation stage. Figure 7 shows that the same optimal interference envelope was recovered by translating the reference mirror by the same distance $\Delta z_r = \Delta z_T = 2.35$ mm (gray points). We chose this specific separation because it corresponded to the envelope width (FWHM) δ that also yields the OCT resolution, defined as the distance between two target peaks where they cross at half-maximum. The spatial resolution δ is related to the spectral bandwidth by $\delta = 0.36\lambda^2/\Delta\lambda_F$.

5. Conclusion

We have presented the development and characterization of amplified spontaneous parametric downconversion and high-gain optical parametric amplification in a single spatial mode based

#113292 - $15.00 USD Received 24 Jun 2009; revised 14 Aug 2009; accepted 16 Sep 2009; published 22 Sep 2009

on type-0 phase matching in PP-MgO:LN. Under pulsed pumping the amplified SPDC signal and idler outputs contained tens of photons per pulse. Pulsed OPA can provide significant gain with modest pump power. We were able to demonstrate an OPA with a gain of nearly 20 dB for an average pump power of 2 W. The high-gain pulsed OPA can be used for phase conjugation and amplification of weak pulses. We have then demonstrated the classical interference arising from the two phase-sensitive cross-correlated beam generated by amplified parametric fluorescence, in a classical OCT interferometer, and calibrated its axial position measurement capability. In particular, we have shown that the use of the SPDC source for OCT is well understood and our theoretical model matches the data correctly. The two parametric devices were developed specifically for implementing a novel OCT technique called phase-conjugate OCT, and our measurements in this work indicate that they are well suited for that purpose. Note that this technology could also be scaled, with higher bandwidth (shorter crystal) and higher energy per pulse (femtosecond pump), to realize efficient all-fiber OCT measurements. In addition, using nondegenerate SPDC for OCT can have the advantage of easily using a signal wavelength optimized for low absorption (such as for biological samples) and then shifting it to the reference wavelength with the OPA for more convenient and efficient detection.

Acknowledgment
This work was supported by the DARPA Quantum Sensors Program.

#113292 - $15.00 USD Received 24 Jun 2009; revised 14 Aug 2009; accepted 16 Sep 2009; published 22 Sep 2009